REPORT

Bi-allelic Mutations in *PKD1L1* Are Associated with Laterality Defects in Humans

Francesco Vetrini,[1] Lisa C.A. D'Alessandro,[2,3] Zeynep C. Akdemir,[4] Alicia Braxton,[1,4] Mahshid S. Azamian,[4] Mohammad K. Eldomery,[4] Kathryn Miller,[5] Chelsea Kois,[5] Virginia Sack,[5] Natasha Shur,[5] Asha Rijhsinghani,[5] Jignesh Chandarana,[1] Yan Ding,[6] Judy Holtzman,[7] Shalini N. Jhangiani,[6] Donna M. Muzny,[6] Richard A. Gibbs,[4,6] Christine M. Eng,[1,4] Neil A. Hanchard,[3,4] Tamar Harel,[4] Jill A. Rosenfeld,[4] John W. Belmont,[4] James R. Lupski,[3,4,6] and Yaping Yang[1,4,*]

Disruption of the establishment of left-right (L-R) asymmetry leads to situs anomalies ranging from situs inversus totalis (SIT) to situs ambiguus (heterotaxy). The genetic causes of laterality defects in humans are highly heterogeneous. Via whole-exome sequencing (WES), we identified homozygous mutations in *PKD1L1* from three affected individuals in two unrelated families. *PKD1L1* encodes a polycystin-1-like protein and its loss of function is known to cause laterality defects in mouse and medaka fish models. Family 1 had one fetus and one deceased child with heterotaxy and complex congenital heart malformations. WES identified a homozygous splicing mutation, c.6473+2_6473+3delTG, which disrupts the invariant splice donor site in intron 42, in both affected individuals. In the second family, a homozygous c.5072G>C (p.Cys1691Ser) missense mutation was detected in an individual with SIT and congenital heart disease. The p.Cys1691Ser substitution affects a highly conserved cysteine residue and is predicted by molecular modeling to disrupt a disulfide bridge essential for the proper folding of the G protein-coupled receptor proteolytic site (GPS) motif. Damaging effects associated with substitutions of this conserved cysteine residue in the GPS motif have also been reported in other genes, namely *GPR56*, *BAI3*, and *PKD1* in human and *lat-1* in *C. elegans*, further supporting the likely pathogenicity of p.Cys1691Ser in PKD1L1. The identification of bi-allelic *PKD1L1* mutations recapitulates previous findings regarding phenotypic consequences of loss of function of the orthologous genes in mice and medaka fish and further expands our understanding of genetic contributions to laterality defects in humans.

Although vertebrates may appear symmetrical when viewed externally, there is marked left-right (L-R) asymmetry in the positioning of almost all the internal organs. The normal arrangement of internal organs is known as situs solitus. Failure to establish normal organ asymmetry along the left-right axis can result in situs inversus totalis (SIT) or situs ambiguous (also known as heterotaxy). SIT is the complete mirror image of situs solitus whereas heterotaxy refers to discordant organ arrangement with reversal of at least one organ relative to the others.[1] In vertebrates, the establishment of L-R asymmetry occurrs during early embryonic development and involves complex signaling transduction cascades and nodal cilia.[2–4] Whereas the activation of *NODAL* in the left lateral plate mesoderm results in normal position of internal organs (situs solitus), the expression of *NODAL* in the right side of the embryo leads to SIT.[4] In SIT, organ concordance is preserved and congenital organ malformation is rare. In contrast, heterotaxy (randomization of organ positioning and organ discordance) arises from bilateral or absent *NODAL* activation.[5] Approximately 80% of individuals with heterotaxy have complex congenital heart disease (CHD).[6] Overall, situs anomalies have a prevalence of 1 in 10,000 live births and account for approximately 3% of complex CHD.[5–7]

The genetic causes of laterality defects in humans are highly heterogeneous. SIT and heterotaxy with complex CHD can be caused by defects in a number of genes including *ZIC3* (MIM: 300265), *CFC1* (MIM: 605194), *MMP21* (MIM: 608416), *GDF1* (MIM: 602880), *NODAL* (MIM: 601265), *LEFTY2* (MIM: 601877), *ACVR2B* (MIM: 602730), and *FOXH1* (MIM: 603621); those genes encode components or modifiers of nodal signaling, a signal transduction pathway that plays an important role in mesoderm and endoderm formation and subsequent organization of L-R axial structures.[2,3,5,8–14] Additionally, rare variants in other genes including *CCDC11* (MIM: 614759), *CRELD1* (MIM: 607170), *MED13L* (MIM: 608771), *SHROOM3* (MIM: 6045700), *MEGF8* (MIM: 604267), *NKX2-5* (MIM: 600584), *NPHP4* (MIM: 607215), and *PKD2* (MIM: 173910) have also been associated with L-R patterning defects.[5,15–20] Furthermore, approximately 50% of individuals with primary ciliary dyskinesia (PCD) have SIT and approximately 6% have heterotaxy.[21] Despite these previous discoveries, our understanding of the genetic basis of this group of developmental disorders remains relatively limited.

Here, we describe the identification of homozygous mutations in the polycystic kidney disease 1 like 1 gene (*PKD1L1* [MIM: 609721]) by WES and Sanger sequencing. The gene has previously been characterized as an important determinant of L-R axis in mouse and medaka fish.[22–25] Three subjects affected with laterality defects

[1]Baylor Genetics, Houston, TX 77030, USA; [2]Division of Cardiology, Texas Children's Hospital, Houston, TX 77030, USA; [3]Department of Pediatrics, Baylor College of Medicine, Houston, TX 77030, USA; [4]Department of Molecular and Human Genetics, Baylor College of Medicine, Houston, TX 77030, USA; [5]Albany Medical Center, Albany, NY 12208, USA; [6]Human Genome Sequencing Center, Baylor College of Medicine, Houston, TX 77030, USA; [7]Genetics Department, Kaiser Permanente Medical Group, San Jose, CA 95123, USA
*Correspondence: yapingy@bcm.edu
http://dx.doi.org/10.1016/j.ajhg.2016.07.011.

Table 1. Summary of Phenotypic and Molecular Data

	Family 1; Subject 1	Family 1; Subject 2	Family 2; Subject 3
Age of diagnosis	prenatal	prenatal	3 weeks
Sex	male	male	female
Cardiac situs	ND	levocardia	dextrocardia
Atrial situs	solitus: normal systemic and pulmonary venous return	ambiguus: IVC, hepatics to L-sided atrium; R-SVC, PV to R-sided atrium	inversus: normal systemic and pulmonary venous connections with mirror image situs
AV valves and ventricles	U-AVSD; LV hypoplasia	U-AVSD; LV hypoplasia	CCTGA; LV hypoplasia; VSD
Great arteries	DORV with malposed great arteries	PA with MAPCAS; R-aortic arch	PA
Abdominal situs	inversus: R-sided stomach, L-sided liver, R-sided spleen	inversus: R-sided stomach, L-sided liver, R-sided spleen	inversus, R-sided stomach, L-sided liver, R-sided spleen
Nucleotide change (Hom)	c.6473+2_6473+3delTG		c.5072G>C
Effect	splice donor site at exon 42/intron 42 boundary		p.Cys1691Ser
Coordinate (Hg19)	chr7: 47,870,812–47,870,813		chr7: 47,886,558
ExAC (Het) (African)	3/10,394		ND
ExAC (Het) (Latinos)	1/11,560		ND
ExAC (Het) (European)	41/66,146		ND
In silico predictions	elimination of the splice donor site (see Figure S1)		SIFT (damaging); MutationTaster (disease-causing); PolyPhen-2 (damaging)

Abbreviations are as follows: CCTGA, congenitally corrected transposition of the great arteries (ventricular inversion); DORV, double outlet right ventricle; ExAC, Exome Aggregation Consortium; Hom, homozygous; Het, heterozygous; IVC, inferior vena cava; L, left; LV, left ventricle; MAPCAS, major aortopulmonary collaterals; ND, no data; PA, pulmonary atresia; PV, pulmonary veins; R, right; SVC, superior vena cava; U-AVSD, unbalanced atrioventricular septal defect; VSD, ventricular septal defect.

from two unrelated families were studied. Subject 1 from family 1 was ascertained from approximately 6,900 consecutive clinical exome case subjects referred to the Exome Laboratory at the Baylor Genetics from November 2011 to December 2015. The similarly affected sibling (subject 2) in family 1 was later recruited and studied by Sanger sequencing. Subject 3 from family 2 was enrolled in the Baylor Hopkins Center for Mendelian Genomics (BHCMG) research study. Written informed consent for all subjects was obtained in accordance with protocols approved by the appropriate human subject ethics committees at Baylor College of Medicine.

WES was completed in the Exome Laboratory at Baylor Genetics (subject 1, father, and mother) and at Baylor College of Medicine Human Genome Sequencing Center (BCM-HGSC) (subject 3) (Table S1). Sequencing and data analyses were conducted as previously described, targeting approximately 20,000 genes, including the coding and the untranslated region (UTR) exons.[26,27] Samples were also analyzed by cSNP array (Illumina HumanExome-12 v1 array) for quality control assessment of exome data, as well as for detecting large copy-number variants (CNVs) and regions of absence of heterozygosity (AOH).[28]

Family 1 is a non-consanguineous family of Northern European ancestry with one fetus (subject 1, II-3) and one deceased child (subject 2, II-2), both affected with heterotaxy and complex CHD, and one healthy child (II-1) (Table 1, Figure 1). The family was referred for prenatal genetic assessment after an ultrasound examination performed at 21 weeks and 6 days of gestation revealed complex congenital malformations of the fetus. The fetus presented with situs ambiguus with atrial situs solitus, unbalanced atrioventricular septal defect with left ventricular hypoplasia, double outlet right ventricle with malposed great arteries, right-sided stomach, left-sided liver, and right-sided spleen (Table 1). The diagnosis was confirmed after birth. The subject expired at 3 weeks of age due to complications of CHD. The family history indicated that a previous child (subject 2) was also diagnosed with heterotaxy. He had atrial situs ambiguus, unbalanced atrioventricular septal defect with left ventricular hypoplasia, pulmonary atresia, right-sided stomach, left-sided liver, and right-sided spleen (Table 1, Figure 1). This child died in the neonatal period due to complications of severe CHD.

Subject 3 (II-1 from family 2) is a 46-year-old female born to consanguineous parents of Iranian origin. She was diagnosed in the first weeks of life with SIT and congenital heart disease including congenitally corrected transposition of the great arteries (ventricular inversion) with a small left ventricle, pulmonary atresia, and ventricular septal defect (Table 1, Figure 1). She underwent placement of a left ventricle to pulmonary artery conduit and ventricular septal defect closure. She has paroxysmal atrial flutter and a dual-chamber pacemaker (Figure 1).

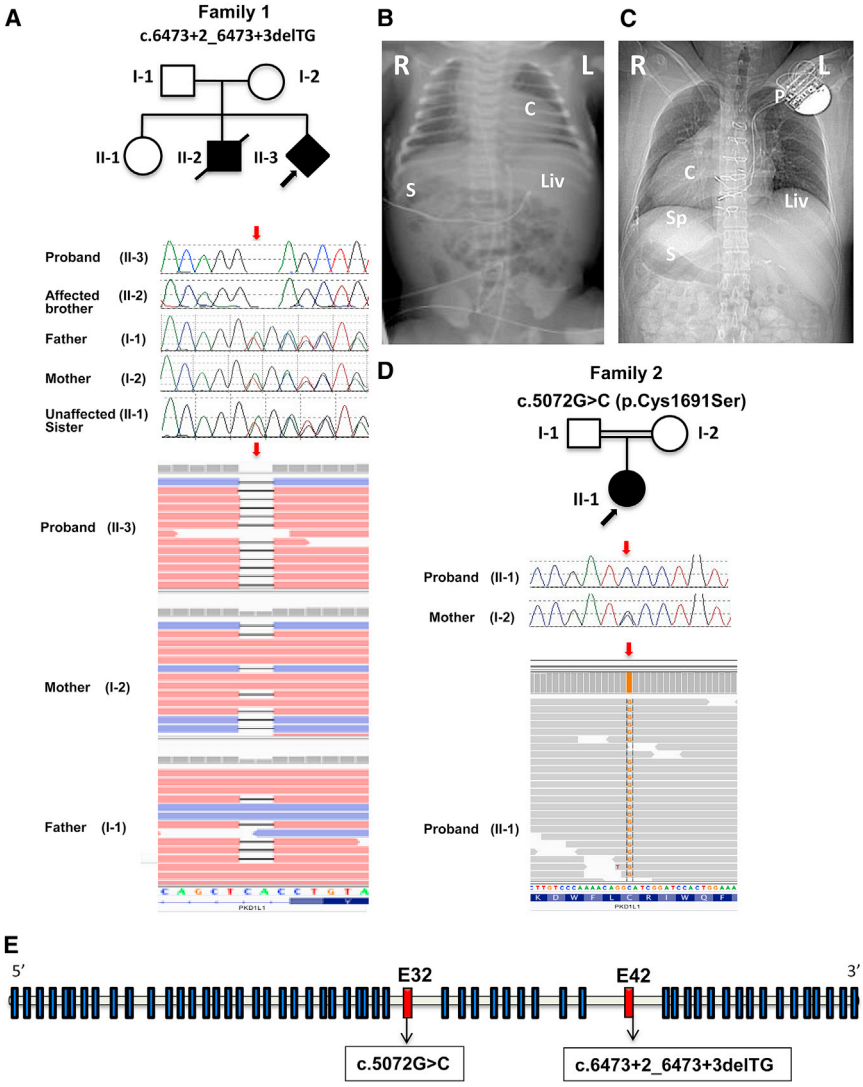

Figure 1. Segregation of *PKD1L1* Mutations with Laterality Defects in Families 1 and 2

(A) NGS reads in Integrative Genomic Viewer (IGV) and Sanger chromatograms show the c.6473+2_6473+3delTG deletion in family 1: proband (II-3, subject 1), affected brother (II-2, subject 2), unaffected sister (II-1), father (I-1), and mother (I-2). The c.6473+2_6473+3delTG deletion is homozygous in the proband and the affected brother and heterozygous in the parents. The mutation is indicated by red arrows.

(B) Plain radiograph of the chest and abdomen of the affected brother in family 1 (subject 2) at birth shows situs ambiguous with levocardia and leftward apex (white "C"), left-sided liver (Liv), right-sided stomach (S); R = right, L = left.

(C) CT localizer radiograph of the proband in family 2 (subject 3) demonstrates situs inversus totalis with dextrocardia and rightward apex (C), left-sided liver (Liv), right-sided stomach (S), and right-sided spleen (Sp). Median sternotomy wires are seen as well as a subcutaneous pacemaker (P) with intravascular leads terminating in the left-sided right atrium and subpulmonary ventricle; R = right, L = left.

(D) NGS reads in IGV and Sanger chromatograms show the c.5072G>C (p.Cys1691Ser) missense change in family 2: proband (II-1, subject 3) and mother (I-2). The c.5072G>C (p.Cys1691Ser) change is homozygous in the proband and heterozygous in the mother. The mutation is indicated by red arrows.

(E) Schematic representation of genomic structure of human *PKD1L1*, where solid blue rectangles indicate exons and the horizontal bars introns. The exons 32 and 42 are colored in solid red and the mutations with their relative position are shown.

Trio exome-sequencing analysis was performed on DNA extracted from cultured fetal amniocytes from subject 1 and blood samples from the parents in family 1. WES analysis did not detect any pathogenic variants in genes previously associated with laterality defects.[5,8–21] However, WES identified a homozygous c.6473+2_6373+3delTG variant affecting the invariant splice donor site at the exon 42/intron 42 junction of *PKD1L1* (GenBank: NM_138295.3) in subject 1; WES also showed that the variant is present in the heterozygous state in both parents, consistent with autosomal-recessive Mendelian expectations (Figure 1, Table 1). The next-generation sequencing (NGS) data revealed the presence of this mutation in 97 out of 97 (97:0) reads in the proband, and 45:63 and 30:58 of the mutation versus the wild-type reads in the mother and the father, respectively (Figure 1, Table 1). In silico programs predicted that the c.6473+2_6473+3delTG variant abolishes the canonical splice donor site in intron 42 (Figure S1), as is usually expected for changes affecting invariant splice sites at the exon-intron boundaries. The minor allele frequency (MAF) of this variant is 0.06% (41/66,146 alleles) in the European non-Finnish population, 0.028% (3/10,394 alleles) in Africans, and 0.008% (1/11,560) in Latinos in the database from the Exome Aggregation Consortium (ExAC; n = 61,486 exomes; accessed February 2016) (Table 1). No homozygotes have been reported for this variant in ExAC. Subsequent Sanger sequencing confirmed the homozygous mutation in the proband, validated the segregation of alleles in both the parents, and showed that the deceased brother was homozygous and the healthy sister was heterozygous for this change (Figure 1). The detection of this variant in homozygous configuration in the proband and the affected brother shows that the homozygous genotype segregates with the congenital malformations in the family and supports a causative role of this variant in the affected individuals.

For family 2, proband WES analysis performed on the DNA sample from subject 3 detected a homozygous c.5072G>C (p.Cys1691Ser) missense mutation in the G protein-coupled receptor proteolytic site (GPS) motif of

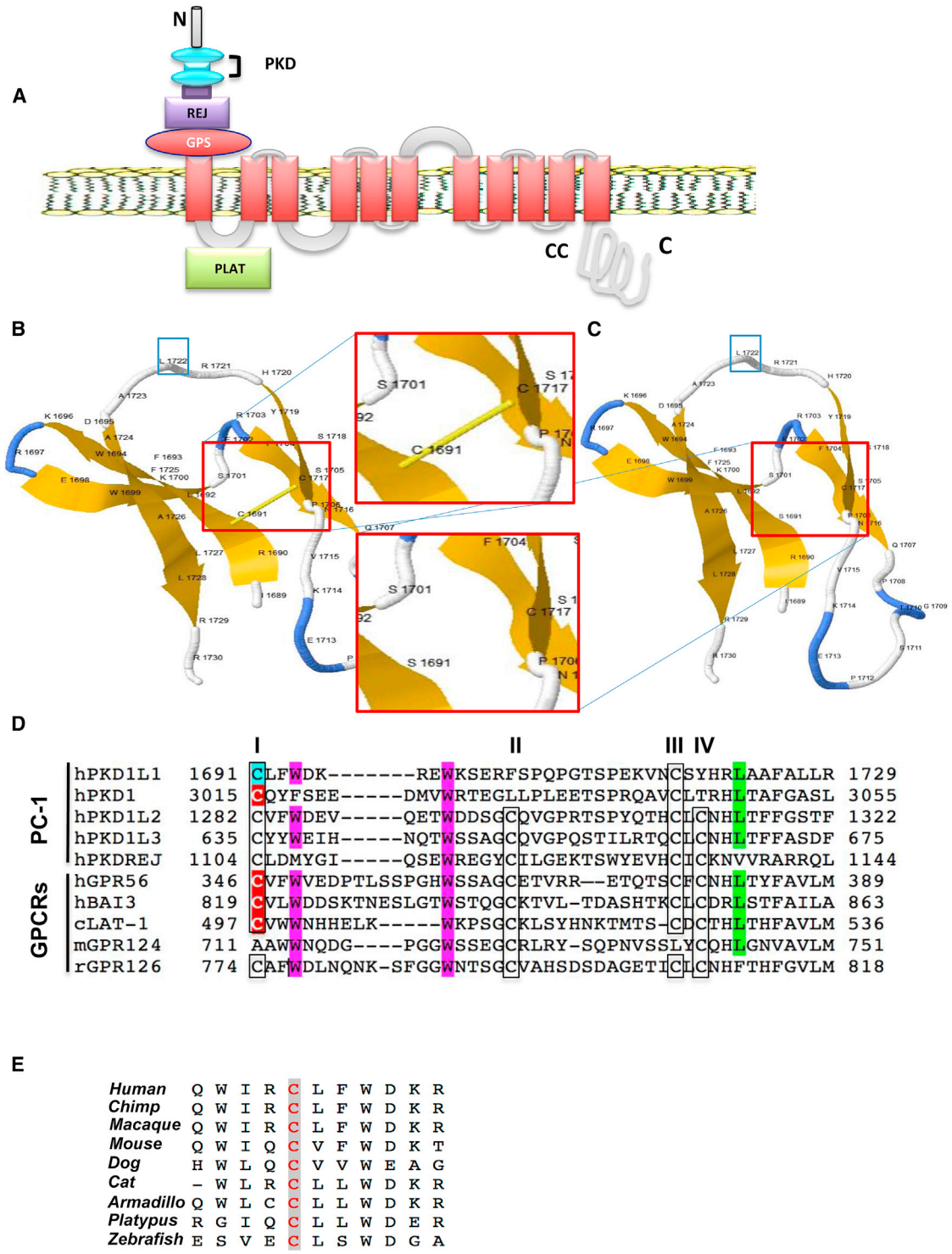

Figure 2. Alignment and Molecular Modeling of the Impact of p.Cys1691Ser Variant on the GPS Motif

(A) Schematic representation of the human PKD1L1 structural domains. PKD1L1 has two Ig-like PKD domains, a REJ domain and a GPS motif in the N-terminal extracellular region, an LH2/Plat domain in the first intracellular loop, and a coiled-coil domain at the C-terminal (CC).

(B and C) 3D models of the GPS motif in PDK1L1 in the wild-type (B) and p.Cys1691Ser mutant (C) by Phyre2 based on the GPS motif in the GAIN and HormR domains of human brain angiogenesis inhibitor 3 (BAI3). The five β strands are shown with numbered amino acids corresponding to the coding sequence of PKD1L1. Cys to Ser substitution at the position 1691 (magnification boxed in red) eliminates the highly conserved disulfide bridge between cysteine residues 1691 and 1717 represented by the yellow solid bar. The conserved Leu1722 residue at the putative cleavage site is boxed in blue.

(D) Alignment of the GPS motif in PKD1L1, other members of PC-1 family, and G protein couple receptors (GPCRs). The GPS motif contains four conserved cysteines arranged in a specific fashion (C-x_2-W-x_{6-16}- W-x_4-C-x-$_{10-22}$-C-x-C) just before the first transmembrane

(legend continued on next page)

PKD1L1 (GenBank: NM_138295.3) (Figure 1, Table 1). The NGS data revealed the presence of this mutation in 110 out of 110 (110:0) reads in the proband; no wild-type reads were identified (Figure 1). This variant is located in exon 32 and affects a cysteine residue that is highly conserved during evolution (Figure 2). The p.Cys1691Ser substitution is predicted to be deleterious by in silico prediction tools (Table 1). This variant is absent from ExAC (n = 61,486 exomes; accessed February 2016). Sanger sequencing confirmed that the variant is homozygous in the proband and also showed that the unaffected mother is heterozygous for the change. The father was not available for study (Figure 1). However, it is likely that the father is heterozygous for the variant since this change is located within a copy-neutral AOH region of approximately 16 Mb (chr7: 40,538,810–56,534,467) in subject 3.

Human *PKD1L1*, which belongs to the polycystin cation channel family 1 (PC-1), is a paralog of *PKD1* (polycystin-1 [MIM: 601313]) and consists of 58 exons spanning 187 kb of genomic DNA. The 2,849-amino acid protein contains in the N-terminal extracellular region two immunoglobulin (Ig)-like polycystic kidney disease (PKD) domains, a small receptor for egg jelly (REJ) domain, a GPS motif, 11 putative transmembrane segments, a polycystin-1, lipoxygenase, alpha-toxin (PLAT) domain, and a C-terminal intracellular coiled-coil (CC) (Figure 2); all the domains can also be found in PKD1. RNA dot-blot analysis of multiple human tissues has demonstrated *PKD1L1* expression in adult and fetal heart and in testis.[29]

Several independent animal models provide evidence for the involvement of *PKD1L1* in the L-R patterning in vertebrates. First, in a *Pkd1l1*$^{-/-}$ mouse model, approximately one-third of the homozygous mutant mice showed situs inversus (SI) without other phenotype or lesions suggestive of underlying primary ciliary dyskinesia (PCD) such as impaired mucociliary clearance or reproductive defects.[23] The *Pkd1l1*$^{-/-}$ mice showed markedly reduced viability during development or early postnatal period. The author hypothesized that undiagnosed CHD associated with laterality defects might be the potential cause, although the hearts and great vessels of these mice were not examined. Second, the *Pkd1l1*$^{rks/rks}$ mutant mice carrying a homozygous p.Asp411Gly substitution, which disrupts a highly conserved PKD domain of PKD1L1, also displayed L-R laterality defects including randomized stomach situs, randomized heart apex, and right lung isomerism. Mutant *Pkd1l1*$^{rks/rks}$ mice showed embryonic lethality by 15.5 dpc.[24] In addition to internal organ discordance, the authors also showed that *Pkd1l1*$^{rks/rks}$ mutants failed to activate the asymmetric gene expression at the node or in the lateral plate.[24] Furthermore, Field and collaborators showed that *Pkd1l1* was exclusively expressed in the node with a spatiotemporal pattern corresponding to the establishment of L-R asymmetry. Ciliary morphology and motility of nodal cells in *Pkd1l1* and *Pkd2* mutants were both normal, suggesting a functional role for the two genes downstream of nodal flow.[24] Additionally, they demonstrated that PKD1L1 interacts through the C-terminal coiled coil (CC) domain with the C-terminal region of PKD2 in the node and hypothesized that PKD1L1 and PKD2 form complexes within cilia that sense nodal flow and are involved in left-sided activation of the Nodal signaling cascade.[24] In a third study,[22] Grimes and collaborators demonstrated that (1) PKD1L1 is required to restrict *Nodal* activation to the left side downstream of nodal flow; (2) PKD1L1 can mediate fluid flow-induced Ca^{+} signal response in vitro, suggesting an analogous role in vivo in the elicitation of nodal flow response; and (3) importantly, the complete loss-of-function *Pkd1l1*$^{tm1/tm1}$ mutant mice presented with randomized laterality of heart and stomach at E13.5. In addition, 43% of the mutants surviving until adulthood exhibited reversed situs. Finally, keeping with the role of *Pkd1l1* in laterality defects in mice, a previous study showed that medaka fish mutant *abecobe* (*abc* is the homolog of *PKD1L1* in humans and *Pkd1l1* in mouse) displays L-R developmental patterning defects, which included randomized direction of heart looping and randomized liver and gallbladder positioning.[25]

Collective data based on animal models, the severity of the variant, and the co-segregation of disease and genotype suggested that the c.6473+2_6473+3delTG *PKD1L1* mutation in subjects 1 and 2 from family 1 is the most parsimonious molecular explanation for these individuals' phenotypic features. In order to further determine the effect of the c.5072G>C (p.Cys1691Ser) variant in family 2, a structural prediction of the extracellular region containing the amino acid change in PKD1L1 was determined using the in silico protein modeling bioinformatics tools Phyre2 and I-TASSER.[30–33] The crystal structures of the GPS motif in the GPCR-autoproteolysis inducing (GAIN) and hormone receptor (HormR) domains of human brain angiogenesis inhibitor 3 (BAI3) and the GAIN and HormR domains of rat CIRL/latrophilin 1 (CL1) were identified by the prediction programs as top-ranked structural analogs and were used as templates for subsequent analyses

domain. The conserved cysteine (C) residues are boxed; the conserved tryptophan (W) residues are highlighted in magenta. The first cysteine residues are numbered with respect to the protein sequence. PKD1L1 and PKD1 do not have the second and fourth (II and IV) cysteine residues in the conserved positions. The putative cleavage site leucine residues that are located in the turn between the last two β strands of the GPS motif are highlighted in green in the alignment. Highlighted in cyan is the mutant site of PKD1L1 GPS in subject 3 (II-1 from family 2) of this study. Highlighted in red are the previously reported mutant sites in the GPS motif in hPKD1, hBAI3, and hGPR56 and cLAT-1. Abbreviations are as follows: h, human; r, rat; m, mouse; c, *C. elegans*.
(E) ClustalW multiple alignment analysis shows high level evolutionary conservation of the human Cys1691 residue in PKD1L1 across multiple species (highlighted in gray).

Table 2. Reported Mutations Affecting the Conserved Cysteine in the GPS Motif

Gene	Residue Position	Variant	Associated Phenotype/ Effect
PKD1L1	c.5072G>C	p.Cys1691Ser	SIT (subject 3, family 2 of this study)
GPR56	c.1036T>A	p.Cys346Ser	bilateral frontoparietal polymicrogyria (BFPP)[36,37]
BAI3	c.2904G>A	p.Cys819Tyr	mutated in non-small cell lung cancer[39]
PKD1	c.9043T>A	p.Cys3015Ser	affects PKD1 cleavage activity in vitro[38]
lat-1	c.1489T>A	p.Cys497Ser	disrupts disulfide bond and affects LAT-1 receptor activity in *C. elegans*[35]

(Figures 2, S2, and S3). The GPS motif serves as an autoproteolytic cleavage site located just before the first trans-membrane domain; this motif is shared by some G protein-coupled receptors (GPCRs) and the polycystin-1 (PC-1) family members (Figure 2).[34] Previous studies showed that the GPS motif is structurally characterized by five β strands that are integrated into the approximately 320-residue GAIN domain.[34,35] The GAIN domain and the ~40-residue GPS motif form a module that is evolutionarily conserved from slime molds to mammals; the module is involved in receptor activation, signaling activity, and intracellular trafficking functions of the GPCRs and PC-1 proteins.[34,35] Three key elements appear to be fundamental for the proper folding and activity of the GPS motif: (1) disulfide bonds between neighboring β strands that enable the formation of the sharp loop between the last two strands containing the conserved leucine at the cleavage site (Figure 2); (2) hydrophobic interaction between the last β strands; and (3) the trapping of the highly conserved leucine within a conserved hydrophobic pocket.[34] Of note, all the members of the PC-1 family share these structural features with the GPCR proteins, although PKD1 and PKD1L1 have only one disulfide bond at the penultimate β strand (Figure 2). GPS autoproteolytic cleavage is essential for protein maturation, intracellular trafficking, and other normal functions of the GPS motif-containing proteins.[34–38] Mutations that alter the GPS structural integrity without affecting autoproteolysis can also abrogate the protein function.[35] Our analysis revealed that p.Cys1691Ser in *PKD1L1* abolishes the essential disulfide bridge between the first and the penultimate β strand (Figures 2 and S3) and is therefore predicted to destabilize the tridimensional structure of the GPS motif with potential detrimental effects on protein function and signaling activity as recently shown.[35] Moreover, the predicted alteration of the loop containing the conserved critical leucine residue Leu1722 (Figure 2) may in turn affect GPS cleavage and the trafficking of the protein to the cytoplasm.[34]

Intriguingly, changes affecting the same conserved residue in the GPS motif corresponding to Cys1691 in *PKD1L1* (residue highlighted in cyan in Figure 2) have been reported in at least three other human genes—*GPR56* (MIM: 604110), *BAI3* (MIM: 602684), and *PKD1* (MIM: 601313)—as well as *latrophilin-1* (*lat-1*) in *C. elegans*, as identified by Domain Mapping of Disease Mutation (DMDM) analysis and literature review (summarized below and in Table 2).[35–40] In one study, a homozygous p.Cys346Ser substitution in GPR56 corresponding to the identical substitution detected in *PKD1L1* has been reported in two subjects with bilateral frontoparietal polymicrogyria (BFPP [MIM: 606854]) (Figure 2); the molecular studies have demonstrated that this change produces a GPR56 protein with dramatically impaired cleavage that fails to traffic beyond the endoplasmic reticulum, with consequent loss of function of the protein.[36,37] Another study showed that the conserved Cys819 in the putative tumor-suppressor gene *BAI3* (Figure 2) is mutated to Tyr in cancer cells and the change is predicted to affect the activity of the protein.[39] Furthermore, it has been shown that in vitro site-specific mutagenesis of Cys to Ser at the position 3015 in PKD1 (Figure 2) affects the cleavage of the protein at the GPS motif.[38] Lastly, a recent study in *C. elegans* showed that the corresponding substitution p.Cys497Ser in the LAT-1 protein (Figure 2) affects the GPS structural integrity by disrupting the normal disulfide bond patterns and results in an inactive receptor.[35] Based on the predictions from molecular modeling that shows that p.Cys1691Ser in PKD1L1 abolishes an essential disulfide bridge, together with the evidence of the damaging effects associated with changes of the conserved cysteine in other genes, we conclude that the homozygous *PKD1L1* c.5072G>C (p.Cys1691Ser) mutation is most likely the cause of the laterality defects in subject 3 from family 2.

PDKD1L1 interacts with PKD2,[22,24,25,41] which is also involved in L-R patterning in mouse, medaka fish, and zebrafish models.[42,43] Additionally, *Pkd1l1*$^{-/-}$ and *Pkd2*$^{-/-}$ mouse mutants phenocopy strongly. However, in humans, *PKD2* heterozygous mutations cause polycystic kidney disease 2 (MIM: 613095), a form of ciliopathy arising from abnormalities of the renal primary cilium. Heterozygous mutations in *PKD2* have also been reported in individuals with laterality defects but the occurrence is rare.[17] Further studies are needed in order to elucidate the role of PKD1L1 and PKD2 in the establishment of left-right body asymmetry in humans and to determine whether additional PKD1L1 partners might be potentially involved in human laterality disorders.

In summary, we identified two homozygous mutations in *PKD1L1* in three individuals who presented with laterality defects. Our findings recapitulate those in mouse and medaka fish and further expand the genetic heterogeneity of laterality defects in humans.

Accession Numbers

The ClinVar accession numbers for the DNA variant data reported in this paper are SCV000280028 and SCV000280029.

Supplemental Data

Supplemental Data include three figures and one table and can be found with this article online at http://dx.doi.org/10.1016/j.ajhg.2016.07.011.

Conflicts of Interest

J.R.L. is a paid consultant for Regeneron Pharmaceuticals, holds stock ownership in 23andMe and Lasergen, Inc., is on the Scientific Advisory Board of Baylor Genetics, and is a co-inventor on United States and European patents related to molecular diagnostics. J.W.B. is currently employed by Illumina, Inc. The Department of Molecular and Human Genetics at Baylor College of Medicine derives revenue from molecular genetic testing offered at the Baylor Genetics.

Acknowledgments

We thank the families for their participation and collaboration. We thank Irene Miloslavskaya, Anh Dang from Baylor Genetics, and Theodore Chiang from Human Genome Center for their technical support. The study was supported in part by the US National Human Genome Research Institute (NHGRI)/National Heart Lung and Blood Institute (NHLBI) grant no. U54HG006542 to the Baylor-Hopkins Center for Mendelian Genomics (J.R.L.). T.H. is supported by the NIH/NIGMS T32 GM07526 Medical Genetics Research Fellowship Program.

Received: April 8, 2016
Accepted: July 11, 2016
Published: September 8, 2016

Web Resources

1000 Genomes, http://www.1000genomes.org
Alamut, http://www.interactive-biosoftware.com/
ClinVar, https://www.ncbi.nlm.nih.gov/clinvar/
Domain Mapping of Disease Mutation, http://bioinf.umbc.edu/DMDM/generatelogo.php?accession=smart00303
ExAC Browser, http://exac.broadinstitute.org/
GenBank, http://www.ncbi.nlm.nih.gov/genbank/
I-TASSER, http://zhanglab.ccmb.med.umich.edu/I-TASSER/
MutationTaster, http://www.mutationtaster.org/
NHLBI Exome Sequencing Project (ESP) Exome Variant Server, http://evs.gs.washington.edu/EVS/
OMIM, http://www.omim.org/
Phyre2, http://www.sbg.bio.ic.ac.uk/phyre2/html/page.cgi?id=index
PolyPhen-2, http://genetics.bwh.harvard.edu/pph2/
RefSeq, http://www.ncbi.nlm.nih.gov/RefSeq
SIFT, http://sift.bii.a-star.edu.sg/
UCSC Genome Browser, http://genome.ucsc.edu

References

1. Raya, A., and Izpisúa Belmonte, J.C. (2006). Left-right asymmetry in the vertebrate embryo: from early information to higher-level integration. Nat. Rev. Genet. *7*, 283–293.
2. Zhou, X., Sasaki, H., Lowe, L., Hogan, B.L., and Kuehn, M.R. (1993). Nodal is a novel TGF-beta-like gene expressed in the mouse node during gastrulation. Nature *361*, 543–547.
3. Collignon, J., Varlet, I., and Robertson, E.J. (1996). Relationship between asymmetric nodal expression and the direction of embryonic turning. Nature *381*, 155–158.
4. Zhu, L., Belmont, J.W., and Ware, S.M. (2006). Genetics of human heterotaxias. Eur. J. Hum. Genet. *14*, 17–25.
5. Sutherland, M.J., and Ware, S.M. (2009). Disorders of left-right asymmetry: heterotaxy and situs inversus. Am. J. Med. Genet. C. Semin. Med. Genet. *151C*, 307–317.
6. Peeters, H., and Devriendt, K. (2006). Human laterality disorders. Eur. J. Med. Genet. *49*, 349–362.
7. Kathiriya, I.S., and Srivastava, D. (2000). Left-right asymmetry and cardiac looping: implications for cardiac development and congenital heart disease. Am. J. Med. Genet. *97*, 271–279.
8. Perles, Z., Moon, S., Ta-Shma, A., Yaacov, B., Francescatto, L., Edvardson, S., Rein, A.J., Elpeleg, O., and Katsanis, N. (2015). A human laterality disorder caused by a homozygous deleterious mutation in MMP21. J. Med. Genet. *52*, 840–847.
9. Guimier, A., Gabriel, G.C., Bajolle, F., Tsang, M., Liu, H., Noll, A., Schwartz, M., El Malti, R., Smith, L.D., Klena, N.T., et al. (2015). MMP21 is mutated in human heterotaxy and is required for normal left-right asymmetry in vertebrates. Nat. Genet. *47*, 1260–1263.
10. Shiraishi, I., and Ichikawa, H. (2012). Human heterotaxy syndrome – from molecular genetics to clinical features, management, and prognosis –. Circ. J. *76*, 2066–2075.
11. Hamada, H., Meno, C., Watanabe, D., and Saijoh, Y. (2002). Establishment of vertebrate left-right asymmetry. Nat. Rev. Genet. *3*, 103–113.
12. Ware, S.M., Harutyunyan, K.G., and Belmont, J.W. (2006). Heart defects in X-linked heterotaxy: evidence for a genetic interaction of Zic3 with the nodal signaling pathway. Dev. Dyn. *235*, 1631–1637.
13. Kaasinen, E., Aittomäki, K., Eronen, M., Vahteristo, P., Karhu, A., Mecklin, J.P., Kajantie, E., Aaltonen, L.A., and Lehtonen, R. (2010). Recessively inherited right atrial isomerism caused by mutations in growth/differentiation factor 1 (GDF1). Hum. Mol. Genet. *19*, 2747–2753.
14. Mohapatra, B., Casey, B., Li, H., Ho-Dawson, T., Smith, L., Fernbach, S.D., Molinari, L., Niesh, S.R., Jefferies, J.L., Craigen, W.J., et al. (2009). Identification and functional characterization of NODAL rare variants in heterotaxy and isolated cardiovascular malformations. Hum. Mol. Genet. *18*, 861–871.
15. Tariq, M., Belmont, J.W., Lalani, S., Smolarek, T., and Ware, S.M. (2011). SHROOM3 is a novel candidate for heterotaxy identified by whole exome sequencing. Genome Biol. *12*, R91.
16. Andersen, T.A., Troelsen, Kde.L., and Larsen, L.A. (2014). Of mice and men: molecular genetics of congenital heart disease. Cell. Mol. Life Sci. *71*, 1327–1352.
17. Bataille, S., Demoulin, N., Devuyst, O., Audrézet, M.P., Dahan, K., Godin, M., Fontès, M., Pirson, Y., and Burtey, S. (2011). Association of PKD2 (polycystin 2) mutations with left-right laterality defects. Am. J. Kidney Dis. *58*, 456–460.
18. Izumi, K., Noon, S., Wilkens, A., and Krantz, I.D. (2014). NKX2.5 mutation identification on exome sequencing in a patient with heterotaxy. Eur. J. Med. Genet. *57*, 558–561.
19. Narasimhan, V., Hjeij, R., Vij, S., Loges, N.T., Wallmeier, J., Koerner-Rettberg, C., Werner, C., Thamilselvam, S.K., Boey, A., Choksi, S.P., et al. (2015). Mutations in CCDC11, which encodes a coiled-coil containing ciliary protein, causes situs inversus due to dysmotility of monocilia in the left-right organizer. Hum. Mutat. *36*, 307–318.

20. Twigg, S.R., Lloyd, D., Jenkins, D., Elçioglu, N.E., Cooper, C.D., Al-Sannaa, N., Annagür, A., Gillessen-Kaesbach, G., Hüning, I., Knight, S.J., et al. (2012). Mutations in multidomain protein MEGF8 identify a Carpenter syndrome subtype associated with defective lateralization. Am. J. Hum. Genet. *91*, 897–905.
21. Knowles, M.R., Daniels, L.A., Davis, S.D., Zariwala, M.A., and Leigh, M.W. (2013). Primary ciliary dyskinesia. Recent advances in diagnostics, genetics, and characterization of clinical disease. Am. J. Respir. Crit. Care Med. *188*, 913–922.
22. Grimes, D.T., Keynton, J.L., Buenavista, M.T., Jin, X., Patel, S.H., Kyosuke, S., Vibert, J., Williams, D.J., Hamada, H., Hussain, R., et al. (2016). Genetic analysis reveals a hierarchy of interactions between polycystin-encoding genes and genes controlling cilia function during left-right determination. PLoS Genet. *12*, e1006070.
23. Vogel, P., Read, R., Hansen, G.M., Freay, L.C., Zambrowicz, B.P., and Sands, A.T. (2010). Situs inversus in Dpcd/Poll-/-, Nme7-/-, and Pkd1l1-/- mice. Vet. Pathol. *47*, 120–131.
24. Field, S., Riley, K.L., Grimes, D.T., Hilton, H., Simon, M., Powles-Glover, N., Siggers, P., Bogani, D., Greenfield, A., and Norris, D.P. (2011). Pkd1l1 establishes left-right asymmetry and physically interacts with Pkd2. Development *138*, 1131–1142.
25. Kamura, K., Kobayashi, D., Uehara, Y., Koshida, S., Iijima, N., Kudo, A., Yokoyama, T., and Takeda, H. (2011). Pkd1l1 complexes with Pkd2 on motile cilia and functions to establish the left-right axis. Development *138*, 1121–1129.
26. Lupski, J.R., Gonzaga-Jauregui, C., Yang, Y., Bainbridge, M.N., Jhangiani, S., Buhay, C.J., Kovar, C.L., Wang, M., Hawes, A.C., Reid, J.G., et al. (2013). Exome sequencing resolves apparent incidental findings and reveals further complexity of SH3TC2 variant alleles causing Charcot-Marie-Tooth neuropathy. Genome Med. *5*, 57.
27. Yang, Y., Muzny, D.M., Xia, F., Niu, Z., Person, R., Ding, Y., Ward, P., Braxton, A., Wang, M., Buhay, C., et al. (2014). Molecular findings among patients referred for clinical whole-exome sequencing. JAMA *312*, 1870–1879.
28. Lalani, S.R., Liu, P., Rosenfeld, J.A., Watkin, L.B., Chiang, T., Leduc, M.S., Zhu, W., Ding, Y., Pan, S., Vetrini, F., et al. (2016). Recurrent muscle weakness with rhabdomyolysis, metabolic crises, and cardiac arrhythmia due to bi-allelic TANGO2 mutations. Am. J. Hum. Genet. *98*, 347–357.
29. Yuasa, T., Venugopal, B., Weremowicz, S., Morton, C.C., Guo, L., and Zhou, J. (2002). The sequence, expression, and chromosomal localization of a novel polycystic kidney disease 1-like gene, PKD1L1, in human. Genomics *79*, 376–386.
30. Kelley, L.A., Mezulis, S., Yates, C.M., Wass, M.N., and Sternberg, M.J. (2015). The Phyre2 web portal for protein modeling, prediction and analysis. Nat. Protoc. *10*, 845–858.
31. Yang, J., Yan, R., Roy, A., Xu, D., Poisson, J., and Zhang, Y. (2015). The I-TASSER suite: protein structure and function prediction. Nat. Methods *12*, 7–8.
32. Yang, J., and Zhang, Y. (2015). Protein structure and function prediction using I-TASSER. Curr. Protoc. Bioinformatics *52*, 1–15.
33. Yang, J., and Zhang, Y. (2015). I-TASSER server: new development for protein structure and function predictions. Nucleic Acids Res. *43* (W1), W174–W181.
34. Araç, D., Boucard, A.A., Bolliger, M.F., Nguyen, J., Soltis, S.M., Südhof, T.C., and Brunger, A.T. (2012). A novel evolutionarily conserved domain of cell-adhesion GPCRs mediates autoproteolysis. EMBO J. *31*, 1364–1378.
35. Prömel, S., Frickenhaus, M., Hughes, S., Mestek, L., Staunton, D., Woollard, A., Vakonakis, I., Schöneberg, T., Schnabel, R., Russ, A.P., and Langenhan, T. (2012). The GPS motif is a molecular switch for bimodal activities of adhesion class G protein-coupled receptors. Cell Rep. *2*, 321–331.
36. Jin, Z., Tietjen, I., Bu, L., Liu-Yesucevitz, L., Gaur, S.K., Walsh, C.A., and Piao, X. (2007). Disease-associated mutations affect GPR56 protein trafficking and cell surface expression. Hum. Mol. Genet. *16*, 1972–1985.
37. Piao, X., Hill, R.S., Bodell, A., Chang, B.S., Basel-Vanagaite, L., Straussberg, R., Dobyns, W.B., Qasrawi, B., Winter, R.M., Innes, A.M., et al. (2004). G protein-coupled receptor-dependent development of human frontal cortex. Science *303*, 2033–2036.
38. Qian, F., Boletta, A., Bhunia, A.K., Xu, H., Liu, L., Ahrabi, A.K., Watnick, T.J., Zhou, F., and Germino, G.G. (2002). Cleavage of polycystin-1 requires the receptor for egg jelly domain and is disrupted by human autosomal-dominant polycystic kidney disease 1-associated mutations. Proc. Natl. Acad. Sci. USA *99*, 16981–16986.
39. Kan, Z., Jaiswal, B.S., Stinson, J., Janakiraman, V., Bhatt, D., Stern, H.M., Yue, P., Haverty, P.M., Bourgon, R., Zheng, J., et al. (2010). Diverse somatic mutation patterns and pathway alterations in human cancers. Nature *466*, 869–873.
40. Peterson, T.A., Adadey, A., Santana-Cruz, I., Sun, Y., Winder, A., and Kann, M.G. (2010). DMDM: domain mapping of disease mutations. Bioinformatics *26*, 2458–2459.
41. Qian, F., Germino, F.J., Cai, Y., Zhang, X., Somlo, S., and Germino, G.G. (1997). PKD1 interacts with PKD2 through a probable coiled-coil domain. Nat. Genet. *16*, 179–183.
42. Pennekamp, P., Karcher, C., Fischer, A., Schweickert, A., Skryabin, B., Horst, J., Blum, M., and Dworniczak, B. (2002). The ion channel polycystin-2 is required for left-right axis determination in mice. Curr. Biol. *12*, 938–943.
43. Bisgrove, B.W., Snarr, B.S., Emrazian, A., and Yost, H.J. (2005). Polaris and Polycystin-2 in dorsal forerunner cells and Kupffer's vesicle are required for specification of the zebrafish left-right axis. Dev. Biol. *287*, 274–288.

The American Journal of Human Genetics, Volume *99*

Supplemental Data

Bi-allelic Mutations in *PKD1L1* Are Associated with Laterality Defects in Humans

Francesco Vetrini, Lisa C.A. D'Alessandro, Zeynep C. Akdemir, Alicia Braxton, Mahshid S. Azamian, Mohammad K. Eldomery, Kathryn Miller, Chelsea Kois, Virginia Sack, Natasha Shur, Asha Rijhsinghani, Jignesh Chandarana, Yan Ding, Judy Holtzman, Shalini N. Jhangiani, Donna M. Muzny, Richard A. Gibbs, Christine M. Eng, Neil A. Hanchard, Tamar Harel, Jill A. Rosenfeld, John W. Belmont, James R. Lupski, and Yaping Yang

Figure S1. Predicted consequences of the variant c.6473+2_6473+3delTG on splicing.

The analysis of the variant was performed by using five predicting tools (SpliceSiteFinder-like, MaxEndScan, NNSPLICE, GeneSplicer and Human Splicing Finder) performed with Alamut Visual of Interactive Biosoftware (http://www.interactive-biosoftware.com/doc/alamut-visual/2.0/splicing.html). In parenthesis are indicated the range of score on the right to the method used. Blue and green vertical bars indicate the predicted 5' and 3' acceptor sites, respectively, with score indicated for those varying between the wild-type and the variant. Sites with scores unchanged between the wild type and the mutated sequence are dimmed. The different predicting tools showed that the c.6473+2_6473+3delTG abolishes the canonical donor splice site.

A

PKD1L1 1690/1722

Rank	PDB Hit	Iden1	Iden2	Cov	Norm. Z-score	
						20 40
						Sec.Str CCCSSSSSSSSSCCCCCCCCCCCCCCCCCCCCSSCCCCCCSSSSSSSCC
						Seq VHFQWIRCLFWDKREWKSERFSPQPGTSPEKVNCSYHRLAAFALLRRK
1	4dloA	0.23	0.25	0.98	1.42	NGTLNPYCVLWDLGTWSTQGCKTV-LTDASHTKCLCDRLSTFAILAQQ
2	4dloA	0.21	0.25	0.98	4.51	NGTLNPYCVLWDDGTWSTQGCKTVLT-DASHTKCLCDRLSTFAILAQQ
3	4dloA	0.23	0.25	0.98	1.31	IELLNPYCVLWDDGTWSTQGCKTVL-TDASHTKCLCDRLSTFAILAQQ
4	4dloA	0.23	0.25	0.98	1.44	NGTLNPYCVLWDLGTWSTQGCKTVL-TDASHTKCLCDRLSTFAILAQQ
5	4dloA	0.24	0.25	0.96	2.07	NGTLNPYCVLWDDGTWSTQGCKTVL-TDASHTKCLCDRLSTFAILAQ-
6	4dloA	0.26	0.25	0.98	1.89	NGTLNPYCVLWDDSEWSTQGCKTVL-TDASHTKCLCDRLSTFAILAQQ
7	4dloA	0.23	0.25	0.98	1.40	NGTLNPYCVLWDLGTWSTQGCKTV-LTDASHTKCLCDRLSTFAILAQQ
8	4dlqA	0.16	0.21	0.79	3.60	KNHFNANCSFWNYGYWSTQGCRLVES-NKTHTTCACSHL---------
9	4dlqA	0.16	0.21	0.79	1.07	FTVFNANCSFWNYGYWSTQGCRLV-ESNKTHTTCACSHL---------
10	4dlqA	0.16	0.21	0.79	1.56	FTVFNANCSFWNYGYWSTQGCRLV-ESNKTHTTCACSHL---------

B

Rank	PDB Hit	TM-score	RMSD	IDEN	Cov
1	4dloA	0.841	1.01	0.234	0.979
2	delqA2	0.643	1.29	0.158	0.792

C

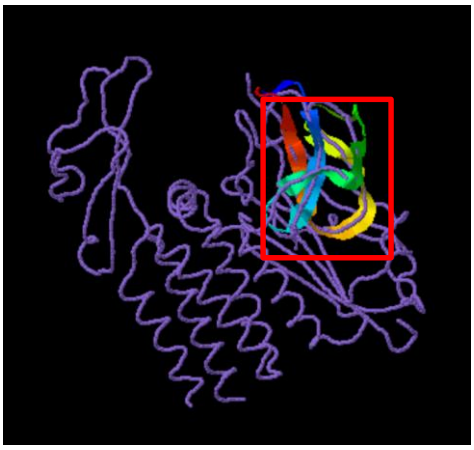

D

Figure S2. ***In silico*** **modeling predictions based on highest ranked identified structural analogs by I-TASSER[1,2,3].**

A) Alignments of PKD1L1 1690 to 1722 protein sequence containing the critical Cys1691 to sequence present in PDB library by I-TASSER which uses TM-align structural alignment program to match the first I-TASSER model to all structures in the PDB library (http://www.rcsb.org/pdb/home/home.do). Rank of templates represents the top ten threading templates used by I-TASSER and are obtained from several programs (1: MUSTER, 2: HHSEARCH2, 3: HHSEARCH I, 4: Neff-PPAS, 5: HHSEARCH, 6:dPPAS , 7: MUSTER, 8: HHSEARCH2, 9: HHSEARCH I , 10: HHSEARCH). GPS motif of GAIN and HormR domains of human brain angiogenesis inhibitor 3 (BAI3) (PDB accession code 4DLO, 1-7 predictions) and GAIN and HormR domains of rat CL1 (PDB accession code, 4DLQ, 8-10 predictions) were identified as the top two structural analogs. Residues in template which are identical to the residue in the query sequence are highlighted in color. PKD1L1 Cys1691 is boxed in red. S= strand; C=coil; Iden1=the percentage sequence identity of the templates in the threading aligned region with the query sequence; Iden2= percentage sequence identity of the whole template chains with query sequence; Cov=coverage of the threading alignment and is equal to the number of aligned residues divided by the length of query protein. Norm. Z-score is the normalized Z-score of the threading alignments. Alignment with a normalized Z-score >1 mean a good alignment and vice versa.

B) Ranking of proteins is based on TM-score (measure of similarity between two protein structures with different tertiary structures) of the structural alignment between the query structure and known structures in the PDB library; RMSD represent root mean square deviation between residues that are structurally aligned by TM-align; IDEN is the percentage sequence identity in the structurally aligned region; Cov represents the coverage of the alignment by TM-align and is equal to the number of structurally aligned residues divided by length of the query protein. TM-score has the value in (0,1), where 1 indicates a perfect match between two structures.

C) Query structure for residues 1690 to 1722 in PKD1L1 using GAIN and HormR domains of human BAI3 model is boxed in red.

D) Query structure for residues 1690 to 1722 in PKD1L1 using GAIN and HormR domains of rat CL1 is boxed in red.

A

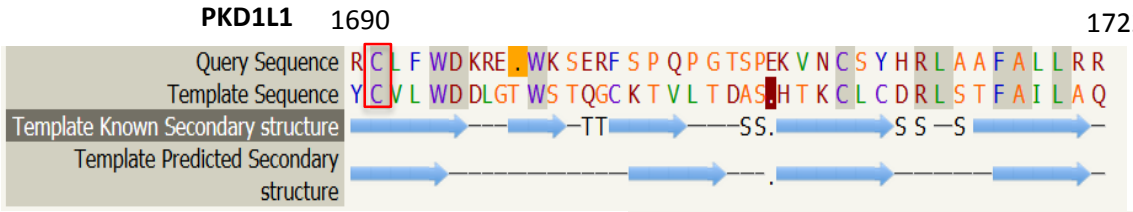
PKD1L1
1690
1722
Query Sequence
Template Sequence
Template Known Secondary structure
Template Predicted Secondary structure

B

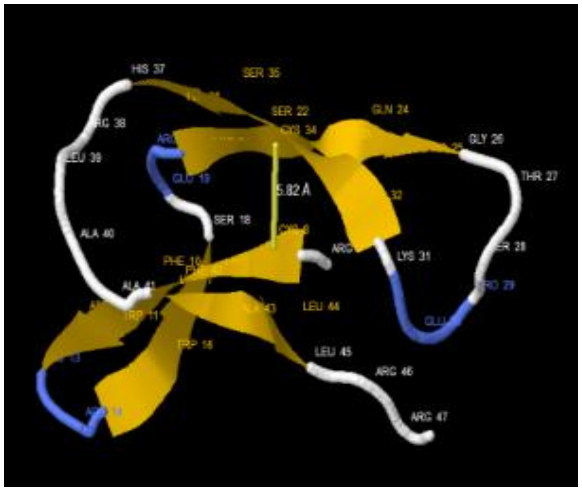

C

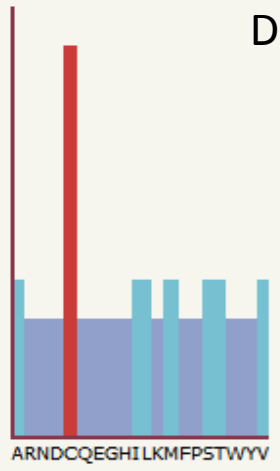
ARNDCQEGHILKMFPSTWYV

D


ARNDCQEGHILKMFPSTWYV

E

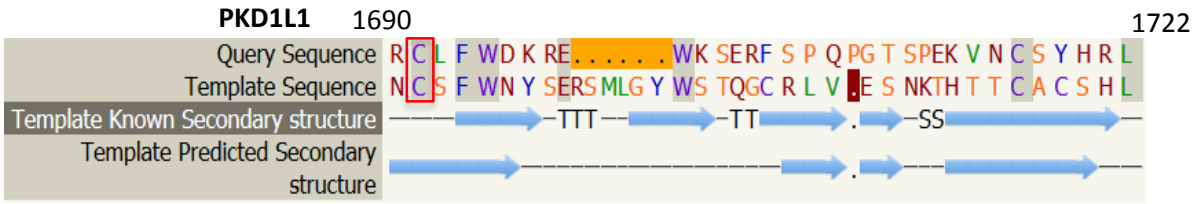
PKD1L1
1690
1722
Query Sequence
Template Sequence
Template Known Secondary structure
Template Predicted Secondary structure

F

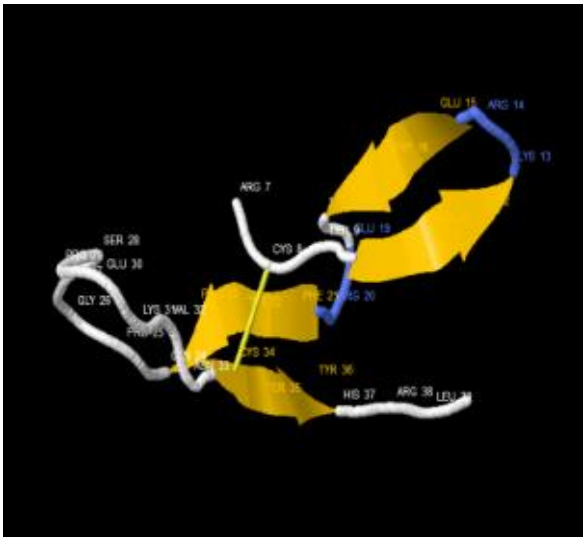

G

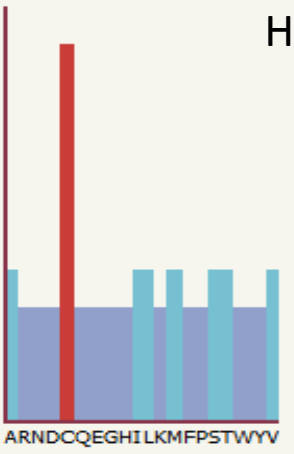
ARNDCQEGHILKMFPSTWYV

H

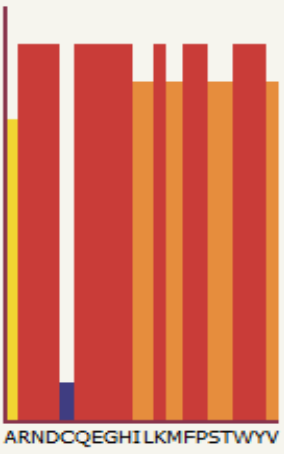
ARNDCQEGHILKMFPSTWYV

Figure S3. ***In silico*** **secondary and 3D structure predictions by Phyre2[4] based on highest ranked models and analysis of the Cys1691 mutation**.

Blue arrows= β-strands; T=hydrogen bonded turn; S=bend. Here the most relevant templates are shown based on the highest structural homology.

A), E) Alignments of PKD1L1 1690 to 1722 protein sequence containing the critical Cys1691 with crystal structures of the GPS motif present in GAIN and HormR domains of human brain angiogenesis inhibitor 3 (BAI3) and GAIN and HormR domains of rat CL1 respectively (PDB accession code 4DLO and 4DLQ respectively). B), F) 3D models showing the critical disulfide bridge between Cys8 (corresponding to the mutated Cys1691 in PKD1L1) and Cys34 (yellow bar).

C), G) Sequence profile graph representing residue preferences in the protein at the position corresponding at Cys1691 of PKD1L1. The twenty possible amino acids are labelled along the x-axis with their one-code letter. The value are calculated by scanning PKD1L1 sequence against a large sequence database using the iterative PSI-blast. The colored bars indicate the favourability of each residue type at the specific position 1691. Tall and red= favorable; short and blue= unfavorable.

D), H) Mutational analysis graph that represents the predicted effect of mutations at the position 1691 in PKD1L1 made by using SuSPect[5] method part of the Phyre2 software package. The twenty possible amino acids are labelled along the x-axis with their one-code letter code. The colored bars indicate the probability that a mutation to the corresponding residue will have a detrimental effect on the protein or the phenotype of the organism; tall and red=likely to affect function, short and blue=unlikely to affect function.

Table S1. WES Sequencing Data of the Probands

Subject	Illumina Platform	Unique Aligned (Mb) [a]	Total Pass filter (Mb) [b]	Avg % Align (PF) Read 1 [c]	Avg % Align (PF) Read 2 [d]	Avg % Error rate Read 1 [e]	Avg % Error rate Read 2 [f]	Unique-ness % [g]	Dupli-cate % [h]	Total Reads Aligned % [i]	Avg Coverage [j]	Reads hit target/ Buffer [k]	Bases 20+ coverage [l]
Subject 1 (629285)	HiSeq 2500	10,650	11,988	95	95	0.54	0.90	93	9.3	61	137	74	98.3
Mother of subject 1	HiSeq 2500	12,068	13,351	95	95	0.41	0.74	92	10.1	64	164	77	98.3
Father of subject 1	HiSeq 2500	11,431	12,431	95	95	0.53	0.92	93	9.2	60	144	73	98.5
Subject 3	HiSeq 2500	10,182.38	10,805	99.16	97.99	0.54	0.83	95.6	6.03	105,454,334	124	77.87	91.61

[a]Unique Aligned (Mbp): the total number of base-pairs in reads that align best to a single location in the reference genome

[b]Total Pass Filter (Mbp): the total number of base-pairs in reads that pass the Illumina quality filters

[c]Avg % Align (PF) Read 1: the average percentage of pass filter base-pairs in Read 1 that align best to a single location in the reference genome

[d]Avg % Align (PF) Read 2: the average percentage of pass filter base-pairs in Read 2 that align best to a single location in the reference genome

[e] Avg % Error rate Read 1: the calculated error rate of bases on Read 1, as determined by aligning to reference genome

[f]Avg % Error rate Read 2: the calculated error rate of bases on Read 2, as determined by aligning to reference genome

[g] Unique-ness %: Percentage of unique reads

[h]Duplicate %: fraction of reads that are identified as duplicate reads – reads whose alignment location is identical to other reads from the same library

[i]Total Reads Aligned: the number of reads that align to the reference genome

[j]Average Coverage: the total number of uniquely aligned bases to the reference genome divided by the size of the reference genome

[k]Reads hit target/buffer: the number of reads whose alignments overlap either a region targeted by the capture reagent, or the 100bp buffer (or both)

[l]Bases 20+ Coverage: the fraction of bases targeted by the capture reagent that are covered by 20 times or more uniquely aligned reads.

References

1.Yang, J., Yan, R., Roy, A., Xu, D., Poisson, J., and Zhang, Y. (2015). The I-TASSER Suite: protein structure and function prediction. Nat Methods 12, 7-8.

2.Yang, J., and Zhang, Y. (2015). Protein Structure and Function Prediction Using I-TASSER. Curr Protoc Bioinformatics 52, 5 8 1-15.

3. Yang, J., and Zhang, Y. (2015). I-TASSER server: new development for protein structure and function predictions. Nucleic Acids Res 43, W174-181.

4. Kelley, L.A., Mezulis, S., Yates, C.M., Wass, M.N., and Sternberg, M.J. (2015). The Phyre2 web portal for protein modeling, prediction and analysis. Nat Protoc 10, 845-858.

5. Yates, C.M., Filippis, I., Kelley, L.A., and Sternberg, M.J. (2014). SuSPect: enhanced prediction of single amino acid variant (SAV) phenotype using network features. J Mol Biol 426, 2692-2701.